Journal of Alloys and Compounds 501 (2010) 301–306

Contents lists available at ScienceDirect

Journal of Alloys and Compounds

journal homepage: www.elsevier.com/locate/jallcom

Characterization and catalytic properties of nano-sized Ag metal catalyst on TiO_2–SiO_2 synthesized by photo-assisted deposition and impregnation methods

R.M. Mohamed [a,b,*], I.A. Mkhalid [a]

[a] Chemistry Department, Faculty of Science, King Abdul Aziz University, Jeddah, Saudi Arabia
[b] Nanostructured Material Division Advanced Materials Department, Central Metallurgical R&D Institute, Helwan, 11421, Cairo, Egypt

ARTICLE INFO

Article history:
Received 9 December 2009
Received in revised form 12 April 2010
Accepted 14 April 2010
Available online 22 April 2010

Keywords:
Nanomaterials
Photocatalysis
Ag-doped titania–silica

ABSTRACT

The photo-assisted deposition (PAD) and impregnation (img) synthesis of nano-sized Ag metal on TiO_2–SiO_2 are reported. The prepared catalysts were characterized by different techniques such as XRD, XAFS, TEM and nitrogen adsorption analysis. Photocatalytic reactivity using Ag–TiO_2–SiO_2 catalysts under visible-light condition on the oxidation of EDTA with O_2 reaction was evaluated. The results have shown notable photocatalytic activity of PAD-Ag–TiO_2–SiO_2 which was 2 and 5 times higher than that of imp-Ag–TiO_2–SiO_2 and TiO_2–SiO_2, respectively.

1. Introduction

TiO_2 photocatalysis is much appreciated in recent years for environmental improvement such as the photodegradation and complete mineralization of organic pollutants [1–5]. TiO_2 nanoparticles have large specific surface areas and high catalytic performance in which reactions take place on the TiO_2 surface. However, their effective commercial applications are hindered by three serious disadvantages. Firstly, agglomerations of ultrafine powders into larger particles result in an adverse effect on catalyst performance. Secondly, the separation and recovery of TiO_2 powders from wastewater are complicated [6,7]. Thirdly, the requirements of ultraviolet (UV) radiation for TiO_2 photocatalysis performance whose energy exceeds the band gap of 3.2 eV (λ = 380 nm) of the anatase crystalline phase, which in turn leads to the utilization of only a very small fraction of sunlight.

More recently, TiO_2 has attracted the attention of scientists in the catalysis field, due to its effective utilization of visible light to degrade organic pollutants. A considerable effort has been devoted to develop supported titania catalysts offering high active surface area, while at the same time having easier separation and removal from wastewater [8,9].

New synthesis methods of titania–silica mixed oxides are needed for overcoming the present disadvantages of pure titania powders. One of the ways is the use of charge-transfer catalysts, which can improve the efficiency of TiO_2. This type can be obtained by the preparation of TiO_2–SiO_2 catalyst with the electron transfer across the solid–solid TiO_2–SiO_2 interface. For that reasons, in a previous study it was reported that the TiO_2–SiO_2 catalyst is 3 times more photoactive than TiO_2 alone [10–12]. Another possibility is to modify TiO_2 by surface deposition of noble metals to shift the process of photodegradation of organic pollutants into the visible-light region [13–16].

Recently, there is much interest in a new nano-sized catalyst such as Pd, Pt, and Au as potentially advanced materials possessing unique electronic, optic and magnetic properties as well as catalytic functions [17–19]. One of the most important factors for controlling catalytic activity of these metal catalysts is the particle size. The development of convenient and useful method to prepare the nano-sized metal loaded on support with controlled particle size and size distribution is an essential task to design a highly active metal catalyst.

On the other hand, Ti-containing mesoporous silica (Ti-HMS) was used as a unique catalyst [21–27]. In Ti-HMS, the tetrahedrally coordinated titanium oxide moieties can be included and isolated within the framework of mesoporous silica. Such transition metal oxides have been named as single-site photocatalysts [21,22]. The single-site photocatalysts including, Ti, Cr, V, and Mo oxide moieties can be incorporated and isolated in the silica matrix of zeolite and can demonstrate the unique photocatalysts [20–30].

Under UV-light irradiation, these single-site photocatalysts generate charge-transfer excited state which can show the highly active and selective photocatalytic performances. In previous studies [21–31], the main focus has been made only on the photocatalytic reactivity but the applications of single-site photocatalyst

* Corresponding author at: Chemistry Department, Faculty of Science, King Abdul Aziz University, Jeddah, Saudi Arabia. Tel.: +966 540715648.
E-mail address: redama123@yahoo.com (R.M. Mohamed).

0925-8388/$ – see front matter © 2010 Elsevier B.V. All rights reserved.
doi:10.1016/j.jallcom.2010.04.092

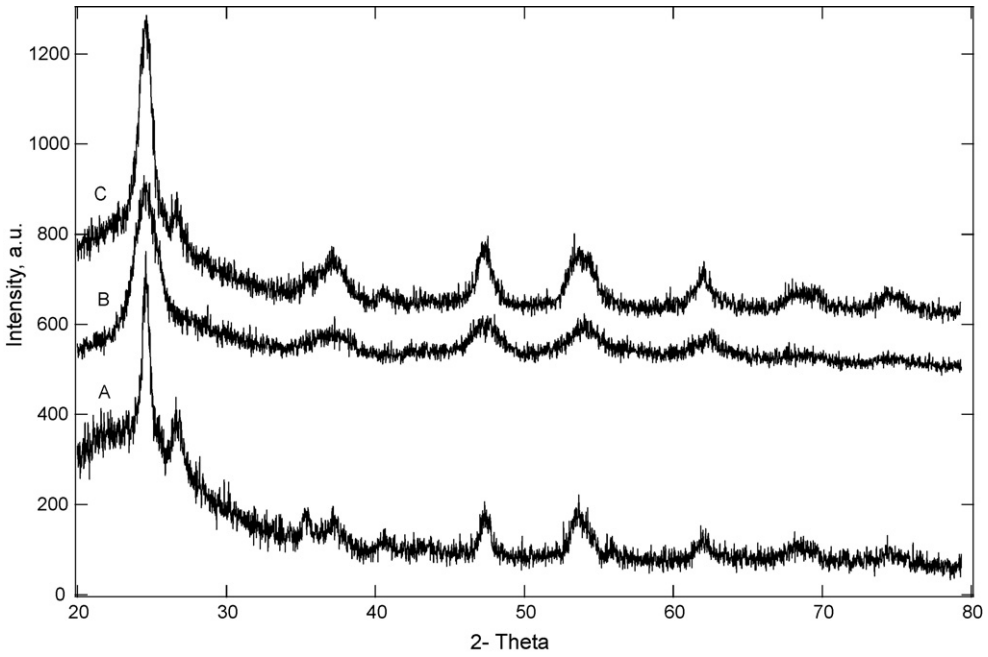

Fig. 1. XRD patterns of the TiO_2–SiO_2 (A), PAD-Ag–TiO_2–SiO_2 (B) and imp-Ag–TiO_2–SiO_2 (C).

for the synthesis of conventional catalysts such as nano-sized metal catalyst have not been yet reported. It can be expected that the metal precursor species can be easily deposited on the excited state of single-site photocatalyst to form well-controlled sized metal particles from the mixture of single-site photocatalyst in the aqueous solution with metal precursor.

In the present study, Ag–TiO_2–SiO_2 was prepared by the application of a photo-assisted deposition (PAD) and impregnation methods. We focus on the photocatalytic reactivity of Ag–TiO_2–SiO_2 for the oxidation of EDTA with O_2.

2. Experimental

2.1. Materials

All chemicals used in this study were used as received without any further purification. Titania–silica mixed oxides were prepared by the hydrolysis of ammonia water (NH_3, 25%). Titanium tetrabutoxide (TBOT, ≥98%) and tetraethyl orthosilicate (TEOS, ≥98%) were selected as the source of titania and silica, respectively. Here, we give a typical procedure for the preparation of titania–silica mixed oxide containing 16.6 mol% silica. 17.0 ml TBOT was mixed with 5.1 ml acetylacetone and 10.0 ml anhydrous ethyl alcohol. Then, 2.25 ml TEOS was mixed with the solution containing 10.8 ml bidistilled water, 23.9 ml ammonia water and 20.0 ml anhydrous ethyl alcohol under stirring. After that, Ti and Si sols were added simultaneously and slowly into the beaker containing 10.0 ml anhydrous ethyl alcohol under stirring. After the above operations, the samples were aged in a beaker covered by a plastic film for 72 h. Finally, the samples obtained were evaporated and dried, followed by calcination at 550 °C for 5 h in air.

On the other side, the Ag loaded on TiO_2–SiO_2 (PAD-Ag–TiO_2–SiO_2, 1 wt% as Ag metal) was prepared using the PAD method: Ag metal was deposited on TiO_2–SiO_2 from aqueous solution of silver nitrate under UV-light irradiation. The Ag loaded on TiO_2–SiO_2 (imp-Ag–TiO_2–SiO_2, 1 wt% as Ag metal) was prepared using the impregnation method: the Ag metal was deposited by a simple impregnation of TiO_2–SiO_2 in the absence of light with aqueous solution of silver nitrate. The samples were dried at 378 K and reduced by H_2 (20 ml min^{-1}) at 473 K for 2 h.

2.2. Characterization techniques

The structure of the catalyst was examined by X-ray diffraction (XRD) on a Rigaku X-ray diffractometer system equipped with as RINT 2000 wide angle Joniometer using Cu Kα radiation and a power of 40 kV × 30 mA. The intensity data were collected at 25 °C over a 2θ range of 20–80°. The UV–vis diffuse reflectance absorption spectra were recorded with a Shimadzu UV-2450 at 295 K. The X-ray absorption fine structure (XAFS) analysis, X-ray absorption near edge structure (XANES) and extended X-ray absorption fine structure (EXAFS) are performed at BL-7C facility [32] of the Photon Factory at the National Laboratory for High-Energy Physics, Tsukuba, Tokyo, Japan. A Si (1 1 1) double crystal was used to monochromatize the X-rays from the 2.5 GeV electron storage ring. The K-edge XAFS spectra of Ag were measured in the fluorescence mode at 298 K. The normalized spectra were obtained by a procedure described in a previous study [33] and Fourier transformed was performed on K^3-weighted EXAFS oscillations in the range of 3–10 $Å^{-1}$. N_2-adsorption measurement was carried out at 77 K using Nova 2000 series, Chromatech. Prior to analysis, the samples were outgased at 250 °C for 4 h. The morphology and particle size of the prepared samples were examined via a transmission electron microscope (Hitachi H-9500 operated at 300 kV).

2.3. Photocatalytic experiments

The photoactivity experiments were carried out in a cylindrical Pyrex glass reactor containing 0.05 g of catalyst and 250 ml of aqueous solution of EDTA at 5×10^{-3} M concentration at 30 °C for 60 min. The sample was then irradiated with a visible light, which was generated by a 150 W high-pressure mercury lamp and an appropriate cut off filter was placed in the front of the reactor to remove the part of UV radiation. The catalysts and solution were separated by filtration and then the resulting solution (EDTA) was determined by comlexometeric titration with Zn^{2+} standard solution. The removal efficiency of EDTA has been calculated by applying the following equation:

$$\%\text{Removal efficiency} = (C^o - C)/C^o \times 100$$

where C^o is the original EDTA content and C is the retained EDTA in solution.

Before all photocatalytic runs, a fresh solution (250 ml) of EDTA was adjusted to the required pH and the catalyst was suspended at 0.2 g/l concentration. Suspensions were kept in dark and magnetically stirred at 30 °C for 60 min. The results indicate that adsorption efficiency was about 15–20%.

3. Results and discussion

3.1. Evaluation and characterization of synthesized material

3.1.1. XRD analysis

XRD patterns of each parent TiO_2–SiO_2 and Ag-doped TiO_2–SiO_2 nanoparticles prepared by imp, and PAD, methods are compared in Fig. 1. The structural characteristic of TiO_2–SiO_2 and all Ag-doped TiO_2–SiO_2, are mainly composed of anatase phase containing a group of lines at 2θ values of 25.2°, 37.5°, 47.7°, 53.3°, 54.7° and 62° [PDF # 71-1169], which indicated that, titania anatase phase structure was maintained after the application of the photo-assisted deposition (PAD) and impregnation methods. However, no diffraction peaks of Ag in the patterns of Ag-doped samples were observed. This is probably attributed to the low Ag doping content (ca. 1%).

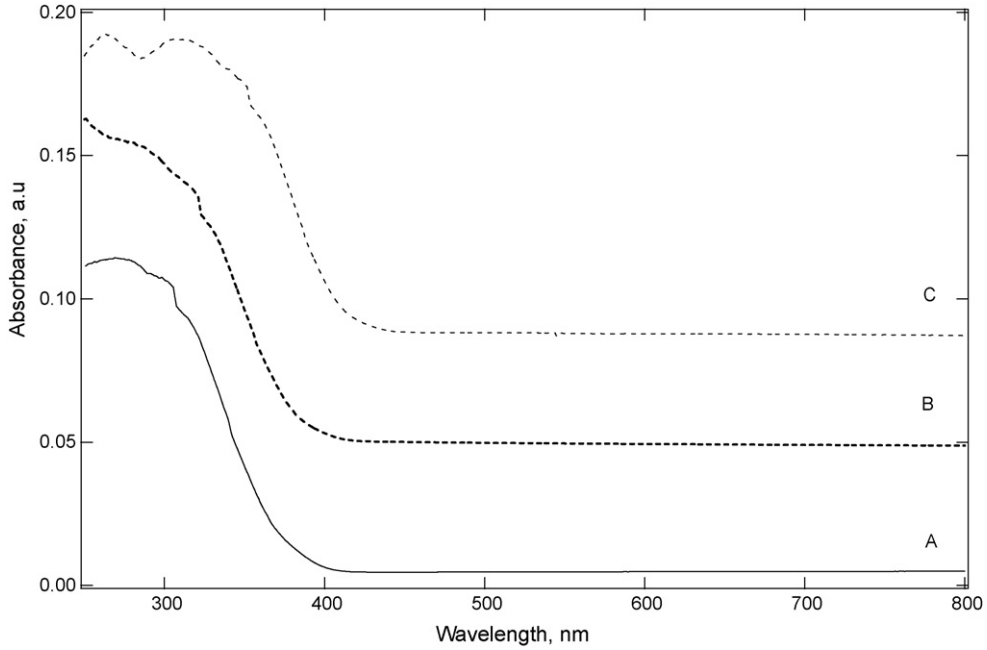

Fig. 2. Diffuse reflectance UV–vis absorption spectra of TiO_2–SiO_2 (A), PAD-Ag–TiO_2–SiO_2 (B) and imp-Ag–TiO_2–SiO_2 (C).

Moreover, the data may imply that, the Ag is well dispersed within the TiO_2–SiO_2 phase.

3.1.2. UV–vis spectroscopy

Fig. 2 depicts the diffuse reflectance UV–vis absorption spectra of TiO_2–SiO_2, PAD-Ag–TiO_2–SiO_2 and imp-Ag–TiO_2–SiO_2. The Kubelka–Munk function, F(R), can be considered to be proportional to the absorption of radiation [22]. On this basis, the value of Eg, the band gap of the semiconductor, can be derived from the spectra by plotting $(F(R)\cdot h\nu)^{1/2}$ against $h\nu$ as shown in Fig. 3 [34]. The Eg values calculated for TiO_2–SiO_2, PAD-Ag–TiO_2–SiO_2 and imp-Ag–TiO_2–SiO_2 are summarized in Table 1. The band-gap values usually reported for pure anatase and rutile phases are 3.2 and 3.03 eV, respectively [35]. However, these values are influenced by the synthesis method, and also affected by the existence of impurities doping the crystalline network and also the average crystal size of the semiconductor. In a previous study, different methods for calculating the Eg from the UV–vis reflectance spectra were used. For example, some authors calculated the Eg values by a direct extrapolation of the F(R) spectrum whereas others reported the wavelength corresponding to the maximum absorption [36]. As a consequence, quite different Eg values for rutile and anatase samples are found in the literature. For instance, for anatase-based materials, the threshold wavelength values of 370 nm [37], 380 nm [38], 387 nm [39], 393 nm [40] and 403 nm have been reported [41] corresponding to a band gap range from 3.08 to 3.35 eV. In the case of rutile-based materials, an absorption wavelength as high as 437.4 nm has been reported (Eg = 2.84 eV) [41]. In the present study, the band gap values calculated for TiO_2–SiO_2, PAD-Ag–TiO_2–SiO_2 and imp-Ag–TiO_2–SiO_2 are 3.2, 3.02 and 2.8 eV, respectively. Therefore, the study of UV–vis radiation absorption constitutes an important tool for the evaluation of the changes produced in the semiconductor materials by different treatments.

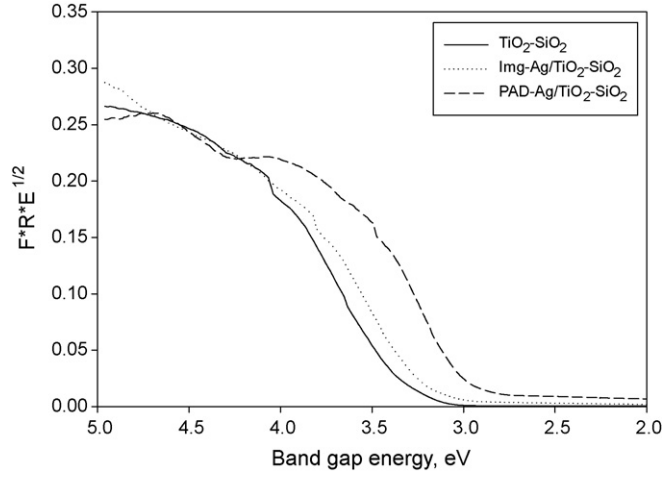

Fig. 3. Band gap calculated from the DR–UV–vis spectra of TiO_2–SiO_2, PAD-Ag–TiO_2–SiO_2 and imp-Ag–TiO_2–SiO_2.

3.1.3. Specific surface area trends

The surface parameters of surface area and the data calculated from the *t*-plot are given in Table 2. The N_2-adsorption isotherms (not shown here) for the parent and the Ag–TiO_2–SiO_2 are typical of mesoporous solids (type IV), however, an increase in the adsorption capacity of the TiO_2–SiO_2 was observed after introducing Ag ions. The surface area changed from 500 (parent TiO_2–SiO_2) to 541 and 652 m^2/g in case of imp-Ag–TiO_2–SiO_2 and PAD-Ag/TiO_2–SiO_2, respectively (≈8.2 and 30.4%, respectively increase of surface area compared to the parent TiO_2–SiO_2). Furthermore, the total pore volume of Ag–TiO_2–SiO_2 is higher than that of TiO_2–SiO_2. The values of S_{BET} and S_t are generally close in most samples indicating the presence of mesopores. The values of S_{meso} are high compared to that of S_{micro} implying that the main surface is mesoporous solid as represented by the isotherm. The surface texture data are correlated with the catalytic activity as will be mentioned later on.

Table 1
The calculated band gap energy of TiO_2–SiO_2, imp-Ag–TiO_2–SiO_2 and PAD-Ag–TiO_2–SiO_2.

Sample	Baud gap energy (eV)
TiO_2–SiO_2	3.20
PAD-Ag–TiO_2–SiO_2	2.80
Imp-Ag–TiO_2–SiO_2	3.02

Table 2
Texture parameters of TiO_2–SiO_2, imp-Ag–TiO_2–SiO_2 and PAD-Ag–TiO_2–SiO_2.

Sample	S_{BET} (m^2/g)	S_t (m^2/g)	S_{micro} (cm^2/g)	S_{meso} (cm^2/g)	S_{ext} (cm^2/g)	V_p (cm^3/g)	V_{micro} (cm^3/g)	V_{meso} (cm^3/g)	r (Å)
TiO_2–SiO_2	500	508	398		396	0.300	0.043	0.257	31.59
Imp-Ag–TiO_2–SiO_2	541	552	430	107	429	0.326	0.055	0.271	30.48
PAD-Ag–TiO_2–SiO_2	652	653	53S	101	546	0.381	0.052	0.329	28.38

Note. S_{BET}: BET-surface area; S_t: surface area derived from V_{l-t} plots; S_{micro}: surface area of micropores; S_{meso}: surface area of micropores; S_{ext}: external surface area; V_p: total pore volume; V_{micro}: pore volume of micropores; V_{meso}: pore volume of mesopores; r: mean pore radius.

3.1.4. EXAFS analysis

The Fourier transforms of Pt LIII-edge EXAFS spectra of the Ag-loaded catalysts are shown in Fig. 4. The presence of the peak assigned to the Ag–Ag bond of Ag metal at around 2.86 Å indicates the formation of nano-sized Ag metal [42]. The intensity of the Ag–Ag peak of the PAD-Ag–TiO_2–SiO_2 catalyst is smaller than the imp-Ag–TiO_2–SiO_2 catalyst. These findings suggest that the size of Ag metal particles depends on the preparation method. Ag metal particles formed on the photo-deposited catalyst (PAD-Ag–TiO_2–SiO_2) show smaller particle size than that of the impregnated catalyst (imp-Ag–TiO_2–SiO_2).

3.1.5. TEM observation

The TEM images of PAD-Ag–TiO_2–SiO_2 and imp-Ag–TiO_2–SiO_2 catalysts are shown in Fig. 5. The particle size distribution obtained from the analysis of TEM images is also shown in Fig. 6. In agree-

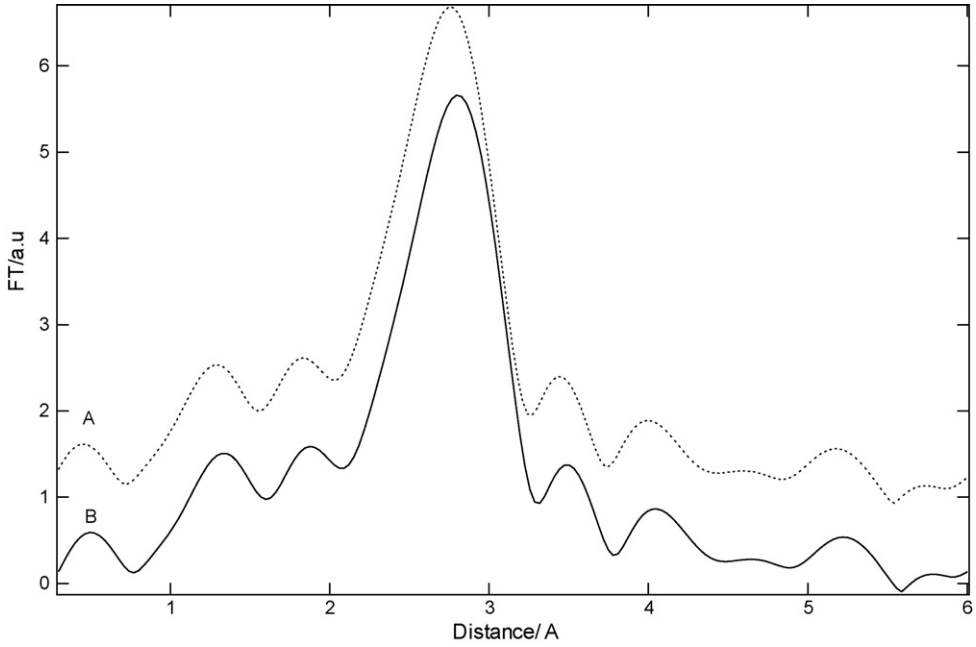

Fig. 4. Fourier transforms of the Pt LIII-edge EXAFS spectra for (A) img-Ag–TiO_2–SiO_2 and (B) PAD-Ag–TiO_2–SiO_2.

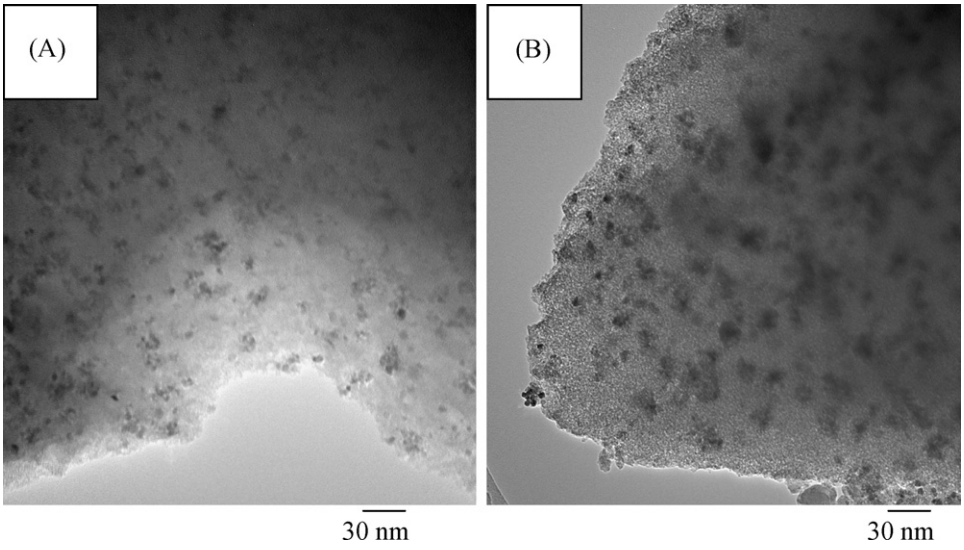

Fig. 5. The TEM images of the PAD-Ag–TiO_2–SiO_2 (A) and imp-Ag–TiO_2–SiO_2 (B) catalyst after H_2 treatment at 473 K.

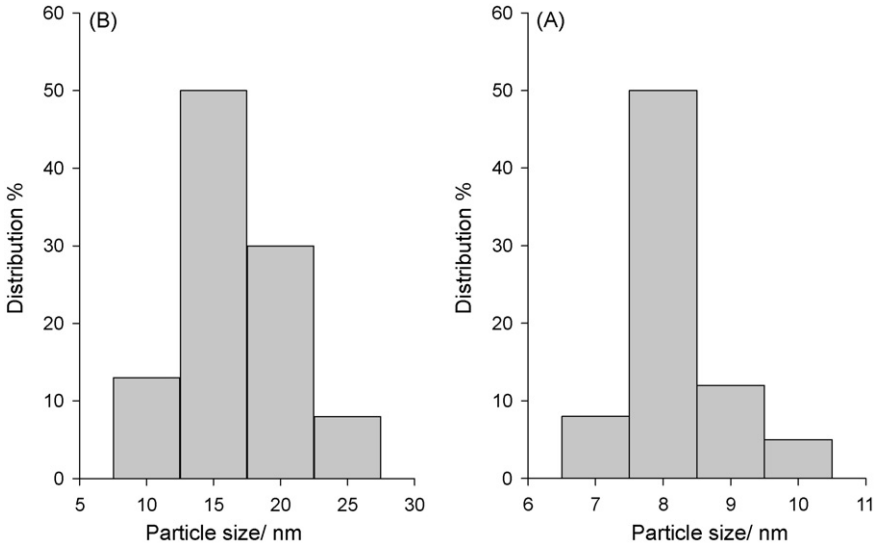

Fig. 6. Size distribution diagrams of Ag metal obtained from the TEM images of the imp-Ag–TiO_2–SiO_2 (A) and PAD-Ag–TiO_2–SiO_2 (B) catalyst after H_2 treatment at 473 K.

ment with the results of XAFS measurement, the nano-sized Ag metal with a mean diameter (d) of ca. 8 nm having a narrow size distribution was found on the PAD-Ag–TiO_2–SiO_2 catalyst, whereas the aggregated Ag metal within various sizes is observed on imp-Ag–TiO_2–SiO_2 catalyst (d = 15 nm).

3.2. Photocatalytic degradation of EDTA

The photocatalytic degradation of EDTA is used as a probe reaction to test the catalytic activity of the prepared nanoparticles. The effect of TiO_2–SiO_2, imp-Ag–TiO_2–SiO_2 and PAD-Ag–TiO_2–SiO_2 on photocatalytic oxidation of EDTA after 6 h at room temperature using 5×10^{-3} M, 25 ml of the EDTA and 50 mg catalyst are shown in Fig. 7. The data demonstrate that the photocatalytic activities of the PAD-Ag–TiO_2–SiO_2 are higher than that of imp-Ag–TiO_2–SiO_2 and parent TiO_2–SiO_2. Considering that, the pure Ag oxides do not have photocatalytic oxidation properties, such variation in activity must be due to the differences in interaction between Ag and TiO_2–SiO_2 that led to several modifications in physical properties such as band gap, particle size and surface texture. Also, we can observe that, the catalytic activity of TiO_2–SiO_2 generally increased with the addition of Ag promoters. A maximum activity was obtained in case of PAD-Ag–TiO_2–SiO_2. The correlation between the photoactivity and the physical properties such as band gap, surface area and pore volume is depicted in Fig. 8. It is clear that, the photocatalytic activity was at a maximum in the case of PAD-Ag–TiO_2–SiO_2 in which the surface area and pore volume were maximum but band gap was minimum. In addition, Fig. 8 shows the good correlation between the band gap, surface area and pore volume with the catalytic activity where the activity is gradually increasing with the decrease of band gap and the increase of the surface area and pore volume.

It is believed that the lack of electron scavengers (surface Ti^{4+}) and hole traps (surface hydroxyl groups) is responsible for the rapid recombination rate of e^-/h^+, which leads to lower photocatalytic activity. The results show that the photocatalytic activities of the

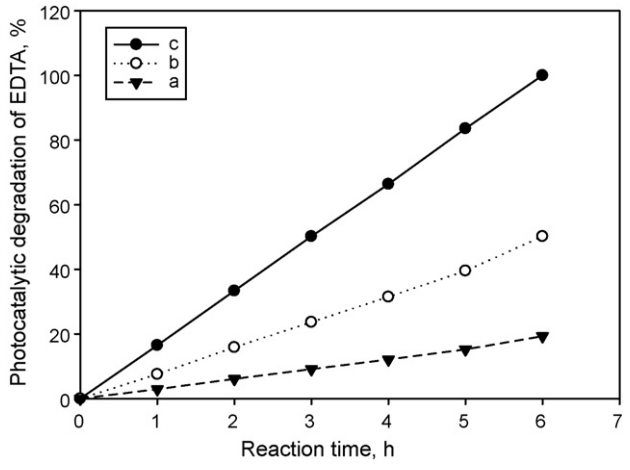

Fig. 7. Photocatalytic degradation of EDTA (%) for (A) TiO_2–SiO_2, (B) imp-Ag–TiO_2–SiO_2 and (C) PAD-Ag–TiO_2–SiO_2.

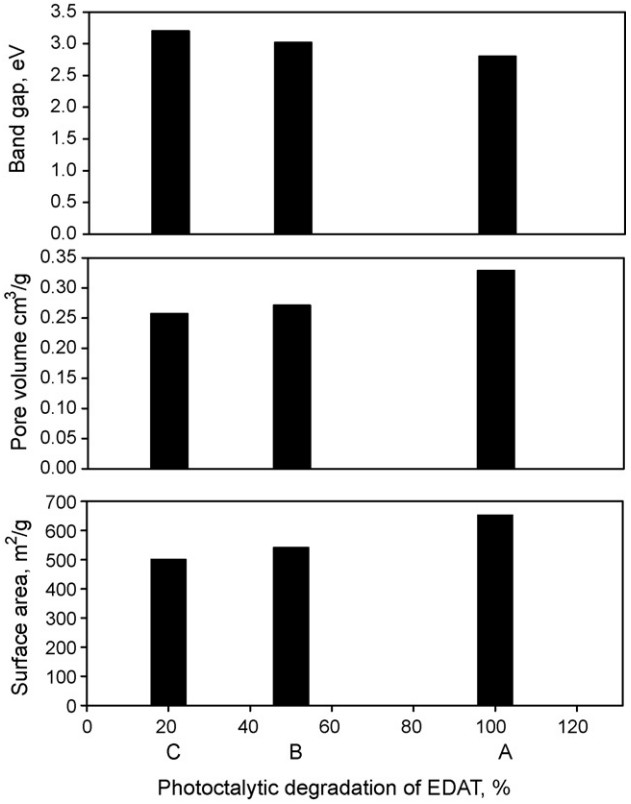

Fig. 8. Effect of physical parameters of the materials on their photocatalytic activity.

Ag-doped TiO_2–SiO_2 nanoparticles increased with decreasing the band gap. This is due to the low energy to exit electron from valance band to conduction band. Also, the PAD-Ag–TiO_2–SiO_2 has the best photoactivity, since it has the lowest band gap and particle size and the highest surface area and pore volume.

4. Conclusions

It can be concluded that the nano-sized particles of Ag–TiO_2–SiO_2 can be prepared via two methods: photo-assisted deposition (PAD) and the conventional impregnation method. The characterization of such prepared catalysts by N_2 adsorption, XRD, UV–vis and XAFS techniques reveals the following remarks:

(1) The nano-sized Ag metal with a mean diameter (d) of ca. 8 nm having a narrow size distribution was found on the PAD-Ag–TiO_2–SiO_2 catalyst, whereas the aggregated Ag metal with various sizes are observed on imp-Ag–TiO_2–SiO_2 catalyst (d = 15 nm).
(2) The calculated values of band gap for TiO_2–SiO_2, PAD-Ag–TiO_2–SiO_2 and imp-Ag–TiO_2–SiO_2 are 3.2, 3.02 and 2.8, respectively.
(3) The N_2-adsorption isotherms for the parent and the Ag–TiO_2–SiO_2 are typical of mesoporous solids, the surface area changed from 500 to 541 and 652 m^2/g in case of imp-Ag–TiO_2–SiO_2 and PAD-Ag–TiO_2–SiO_2, respectively.
(4) The intensity of the Ag–Ag peak of the PAD-Ag–TiO_2–SiO_2 catalyst is smaller than the imp-Ag–TiO_2–SiO_2 catalyst. These findings suggest that the size of Ag metal particles depends on the preparation method. Ag metal particles formed on the photo-deposited catalyst (PAD-Ag–TiO_2–SiO_2) show smaller particle sizes than those obtained from the impregnated catalyst (imp-Ag–TiO_2–SiO_2).

References

[1] A. Linsebigler, G. Lu, J.T. Yates, Chem. Rev. 95 (1995) 735.
[2] A. Fujishima, N.T. Rao, D.A. Rryk, J. Photochem. Photobiol. C: Rev. 1 (2000) 1.
[3] Y. Zhao, C. Li, X. Liu, F. Gu, J. Alloys Compd. 440 (2007) 281.
[4] H. Xia, H. Zhuang, D. Xiao, T. Zhang, J. Alloys Compd. 465 (2008) 328.
[5] Y. Yan, X. Qiu, H. Wang, L. Li, X. Fu, L. Wu, G. Li, J. Alloys Compd. 460 (2008) 491.
[6] J.B. Christophe, A. Francine, C. Pascal, J. Marie, L. Frank, Ceram. J. Am. Soc. 80 (1997) 3157.
[7] Y. Zhu, L. Zhang, W. Yao, L. Cao, Appl. Surf. Sci. 158 (2000) 32.
[8] P.T. Tanev, M. Chibwe, T.J. Pinnavaia, Nature 368 (1994) 321.
[9] J.V. Walker, M. Morey, H. Carlsson, A. Davidson, G.D. Stucky, A.J. Butler, Chem. J. Am. Soc. 119 (1997) 6921.
[10] A.J. Anderson, A.J. Bard, Phys. J. Chem. 99 (1995) 9882.
[11] S.A. Ruetten, J.K. Thomas, Photochem. Photobiol. Sci. 2 (2003) 1018.
[12] H. Chun, Y. Wang, H. Tang, Appl. Catal. B: Environ. 30 (2001) 277.
[13] C.Y. Wang, C.Y. Liu, X. Zheng, Colloids Surf. A: Physicochem. Eng. Aspects 131 (1998) 271.
[14] J.C. Yang, Y.C. Kim, Y.G. Shul, Appl. Surf. Sci. 121 (1997) 525.
[15] H. Kisch, L. Zang, C. Lange, W.F. Maier, C. Antonius, D. Meissner, Angew. Chem. Int. Ed. 37 (1998) 3034.
[16] F.B. Li, X.Z. Li, Appl. Catal. A: Gen. 228 (2002) 15.
[17] K. Mori, T. Hara, T. Mizugaki, K. Ebitani, K. Kaneda, J. Am. Chem. Soc. 126 (2004) 10657.
[18] A. Fukuoka, H. Araki, J. Kimura, Y. Sakamoto, T. Higuachi, N. Sugimoto, S. Inagaki, M. Ichikawa, J. Mater. Chem. 14 (2004) 752.
[19] F. Boccuzzi, A. Chiorino, M. Manzoli, P. Lu, T. Akita, S. Ichikawa, M. Haruta, J. Catal. 202 (2002) 256.
[20] M. Anpo, J.M. Thomas, Chem. Commun. (2006) 3273.
[21] H. Yamashita, M. Anpo, Curr. Opin. Solid State Mater. Sci. 7 (2004) 471.
[22] M. Anpo, M. Che, Adv. Catal. 44 (1999) 119.
[23] H. Yamashita, K. Ikeue, T. Takewaki, M. Anpo, Top. Catal. 18 (2002) 95.
[24] K. Ikeue, H. Yamashita, T. Takewaki, M. Anpo, J. Phys. Chem. B 201 (2001) 8350.
[25] M. Anpo, H. Yamashita, Y. Ichihashi, Y. Fujii, M. Honda, J. Phys. Chem. B 101 (1997) 2632.
[26] M. Anpo, H. Yamashita, Y. Ichihashi, M. Anpo, M. Hasimoto, C. Louis, M. Che, J. Phys. Chem. 100 (1996) 16041.
[27] H. Yamashita, K. Yoshizawa, M. Ariyuki, S. Higashimoto, M. Che, M. Anpo, Chem. Commun. (2001) 435.
[28] C. Murata, H. Yoshida, T. Hattori, Chem. Commun. (2001) 2412.
[29] F. Amano, T. Yamaguchi, T. Tanaka, J. Phys. Chem. B 109 (2006) 281.
[30] N. Ichikuni, H. Murayama, K.K. Bando, S. Shimazu, T. Uematsu, Anal. Sci. 17 (2001) 1193.
[31] R.M. Mohamed, J. Mater. Proc. Technol. 209 (2009) 577.
[32] N. Masaharu, K. Atsushi, J. Synchrotron Radiat. 6 (1999) 182.
[33] C. Anderson, A.J. Bard, J. Phys. Chem. B 101 (1997) 2611.
[34] G. Lassaleta, A. Fernaandez, J.P. Espinoos, A.R. Gonzaolez-Elipe, J. Phys. Chem. 99 (1995) 1848.
[35] M. Schiavello (Ed.), Heterogeneous Photocatalysis, Wiley Chichester, 1997.
[36] R.J. Davis, Z. Liu, Chem. Mater. 9 (1997) 2311.
[37] D.F. Ollis, Catal. Technol. 2 (1998) 149.
[38] K. Kosuge, S. Singh, J. Phys. Chem. B 18 (1999) 3563.
[39] A.A. Belhekar, S.V. Awate, R. Anand, Catal. Commun. 3 (2002) 453.
[40] B.J. Aronson, C.F. Blanford, A. Stein, Chem. Mater. 9 (1997) 2842.
[41] S. Cheng, S. Tsai, Y. Lee, Catal. Today 26 (1995) 87.
[42] P.R. Sarode, K.R. Priolka, B. Bera, M.S. Hegda, S. Emura, R. Kumashiro, Mater. Res. Bull. 37 (2002) 1679.